EPJ manuscript No.
(will be inserted by the editor)

Measurement of charged pions in ^{12}C + ^{12}C collisions at 1 and 2A GeV with HADES

G. Agakishiev[8], C. Agodi[1], A. Balanda[3,V], G. Bellia[1,I], D. Belver[15], A. Belyaev[6], J. Bielcik[4], A. Blanco[2], A. Bortolotti[9]; J. L. Boyard[13], P. Braun-Munzinger[4], P. Cabanelas[15], S. Chernenko[6], T. Christ[11], R. Coniglione[1], M. Destefanis[8], J. Díaz[16], F. Dohrmann[5], I. Durán[15], A. Dybczak[3], T. Eberl[11], L. Fabbietti[11], O. Fateev[6], R. Ferreira-Marques[2,III], P. Finocchiaro[1], P. Fonte[2,II], J. Friese[11], I. Fröhlich[7], T. Galatyuk[4], J. A. Garzón[15], R. Gernhäuser[11], A. Gil[16], C. Gilardi[8], M. Golubeva[10], D. González-Díaz[4], E. Grosse[5], F. Guber[10], M. Heilmann[7], T. Heinz[4], T. Hennino[13], R. Holzmann[4], A. Ierusalimov[6], I. Iori[9,IV], A. Ivashkin[10], M. Jurkovic[11], B. Kämpfer[5], K. Kanaki[5], T. Karavicheva[10], D. Kirschner[8], I. Koenig[4], W. Koenig[4], B. W. Kolb[4], R. Kotte[5], A. Kozuch[3,V], A. Krása[14], F. Křížek[14], R. Krücken[11], W. Kühn[8], A. Kugler[14], A. Kurepin[10], J. Lamas-Valverde[15], S. Lang[4], J. S. Lange[8], K. Lapidus[10], L. Lopes[2], M. Lorenz[7], L. Maier[11], C. Maiolino[1], A. Mangiarotti[2], J. Marín[15], J. Markert[7], V. Metag[8], B. Michalska[9], J. Michel[7], E. Morinière[13], J. Mousa[12] [a], M. Münch[4], C. Müntz[7], L. Naumann[5], R. Novotny[8], J. Otwinowski[3], Y. C. Pachmayer[7], M. Palka[4], Y. Parpottas[12], V. Pechenov[8], O. Pechenova[8], T. Pérez Cavalcanti[8], P. Piattelli[1], J. Pietraszko[4], V. Pospíšil[14], W. Przygoda[3,e], B. Ramstein[13], A. Reshetin[10], M. Roy-Stephan[13], A. Rustamov[4], A. Sadovsky[10], B. Sailer[11], P. Salabura[3], P. Sapienza[1], A. Schmah[11], C. Schroeder[4], E. Schwab[4], R. Simon[4], Yu.G. Sobolev[14], S. Spataro[8], B. Spruck[8], H. Ströbele[7], J. Stroth[7,4], C. Sturm[7], M. Sudol[13], A. Tarantola[7], K. Teilab[7], P. Tlustý[14] [b], M. Traxler[4], R. Trebacz[3], H. Tsertos[12], V. Wagner[14], M. Weber[11], M. Wisniowski[3], T. Wojcik[3], J. Wüstenfeld[5], S. Yurevich[4], Y. Zanevsky[6], P. Zhou[5], P. Zumbruch[4]

[1] Istituto Nazionale di Fisica Nucleare - Laboratori Nazionali del Sud, 95125 Catania, Italy

[2] LIP-Laboratório de Instrumentação e Física Experimental de Partículas , 3004-516 Coimbra, Portugal

[3] Smoluchowski Institute of Physics, Jagiellonian University of Cracow, 30-059 Kraków, Poland

[4] Gesellschaft für Schwerionenforschung mbH, 64291 Darmstadt, Germany

[5] Institut für Strahlenphysik, Forschungszentrum Dresden-Rossendorf, 01314 Dresden, Germany

[a] e-mail: mousa@ucy.ac.cy

[b] e-mail: tlusty@ujf.cas.cz

[6] Joint Institute of Nuclear Research, 141980 Dubna, Russia

[7] Institut für Kernphysik, Johann Wolfgang Goethe-Universität, 60438 Frankfurt, Germany

[8] II. Physikalisches Institut, Justus Liebig Universität Giessen, 35392 Giessen, Germany

[9] Istituto Nazionale di Fisica Nucleare, Sezione di Milano, 20133 Milano, Italy

[10] Institute for Nuclear Research, Russian Academy of Science, 117312 Moscow, Russia

[11] Physik Department E12, Technische Universität München, 85748 München, Germany

[12] Department of Physics, University of Cyprus, 1678 Nicosia, Cyprus

[13] Institut de Physique Nucléaire (UMR 8608), CNRS/IN2P3 - Université Paris Sud, F-91406 Orsay Cedex, France

[14] Nuclear Physics Institute, Academy of Sciences of Czech Republic, 25068 Rez, Czech Republic

[15] Departamento de Física de Partículas, University of Santiago de Compostela, 15782 Santiago de Compostela, Spain

[16] Instituto de Física Corpuscular, Universidad de Valencia-CSIC, 46971 Valencia, Spain

[I] Also at Dipartimento di Fisica e Astronomia, Università di Catania, 95125 Catania, Italy

[II] Also at ISEC Coimbra, Coimbra, Portugal

[III] Also at Universidade de Coimbra, Coimbra, Portugal

[IV] Also at Dipartimento di Fisica, Università di Milano, 20133 Milano, Italy

[V] Also at Panstwowa Wyzsza Szkola Zawodowa , 33-300 Nowy Sacz, Poland

Received: August 11, 2008/ Revised version: August 11, 2008

Abstract. We present the results of a study of charged-pion production in ^{12}C + ^{12}C collisions at incident beam energies of 1 and 2A GeV using the HADES spectrometer at GSI. The main emphasis of these experiments is put on the dielectron signal from the early phase of the collision. Here we discuss the data with respect to the emission of charged hadrons, specifically the production of $\pi^{\pm}$ mesons, which are related to neutral pions representing a dominant contribution to the dielectron yield. We have performed the first large-angular range measurement of the distribution of $\pi^{\pm}$ mesons for the C+C collision system covering a fairly large rapidity interval. The results on yields, transverse mass and angular distributions are compared with calculations with a transport model as well as with existing data from other experiments. The anisotropy is systematically analyzed.

PACS. 25.75.-q heavy-ion collisions - 25.75.Dw charged pion spectra

1 Introduction

The investigation of nuclear matter under the extreme conditions of high temperature and high density is one of the major research topics in modern nuclear physics [1]. Nucleus-nucleus collisions at relativistic energies offer the unique possibility to create such highly excited nuclear matter in the laboratory. The study of particle production as function of beam energy, system size and the centrality of the collisions has been instrumental in the past for understanding the approach towards equilibrium and flow phenomena, as well as for gaining information about the equation of state. Collisions of the light ^{12}C+^{12}C system represent a link between the elementary proton-proton reaction and the heavy-ion collisions of large nuclei. Important physics issues in this context are the degree of thermalization achieved, the role of the mean field and collective motion.

In the few-GeV energy range pions are the only abundantly produced mesons. In heavy-ion collisions their spectra and yields are affected by collective effects like thermalization, directed and elliptic flow, as well as by possible modifications of the properties of the baryon resonances they decay from, in particular the Δ [2,3]. The subtle interplay of the phenomena which change the characteristics of pion production with respect to nucleon-nucleon (N-N) interactions is indeed a challenge to theoretical descriptions. Transport models, in particular, have difficulties in reproducing precisely the experimental data. For a recent comprehensive discussion of various differential pion observables and their comparison with model calculations in the region of 1A GeV see [4].

The High Acceptance DiElectron Spectrometer (HADES) [5], in operation at the heavy-ion synchrotron SIS18 at GSI, Darmstadt, is designed for high-resolution and high-acceptance dielectron spectroscopy in hadron-hadron, hadron-nucleus, and nucleus-nucleus reactions at beam energies in the range from 1 to 2A GeV. Being a charged particle detector, it is of course also an efficient device for hadron detection. First results from HADES on dielectron production in ^{12}C + ^{12}C have been presented in [6,7]. These rely on a precise knowledge of the differential yields of neutral pions, which are the source of the bulk of the detected dielectron pairs, namely the π^0 Dalitz and photon decays. In these analyses the π^0 yields were inferred from those of the charged pions measured by HADES in the same samples of ^{12}C + ^{12}C collisions.

In the present paper we present detailed data on charged pions obtained from ^{12}C + ^{12}C collisions at 1 and 2A GeV. For the first time large intervals of rapidity ($\approx \pm 0.8$ in y/y_{beam} for 2A GeV) and of centre-of-mass angle ($-0.7 < \cos(\theta) < 0.7$) are covered. Our results are compared to transport-model predictions and experimental data from other experiments.

2 Experiment

HADES [5] is a magnetic spectrometer designed as second-generation device for measurements of e^+e^- pairs. The spectrometer, schematically depicted in Fig. 1, is segmented into six identical sectors that cover polar angles between

18 and 85 degrees. Its large (nearly 2π) azimuthal acceptance covers between 65% and 90% of 2π at small and large polar angles, respectively. The analysis of charged pions presented here is based on the same detectors as used in [6,7]. A fast hadron-blind Ring Imaging CHerenkov counter (RICH) is used for electron and positron identification. Four planes of Multi-wire Drift Chambers (MDC1 - MDC4), together with a superconducting magnet, form the magnetic spectrometer for track reconstruction and momentum determination. In the region behind the magnetic field, a set of electromagnetic PreShower detectors (at polar angles $18^\circ - 45^\circ$) [8] and a time-of-flight wall [9] are installed which form the META (Multiplicity and Electron Trigger Array). The time-of-flight detector wall is subdivided into 2 regions: TOF (at polar angles $45^\circ - 85^\circ$) consisting of 384 scintillator slabs of varying length, which are read out at both ends with a time-of-flight resolution of $\sigma = 150$ ps, and TOFINO (at polar angles $18^\circ - 45^\circ$) consisting of 24 scintillator plates read-out on one end with a time-of-flight resolution of $\sigma = 450$ ps. The TOFINO is placed directly in front of the Pre-Shower detector, which provides precise position measurement. The TOF/TOFINO detectors are also used for fast charged-particle multiplicity measurements. Together with the PreShower detectors they provide additional lepton/hadron discrimination power and track coordinate measurements with a spatial resolution in the range from 14 to 25 mm.

A fast data acquisition system is used together with a two-level trigger scheme [10,11]: (a) LVL1 is based on a fast determination of the charged-particle multiplicity

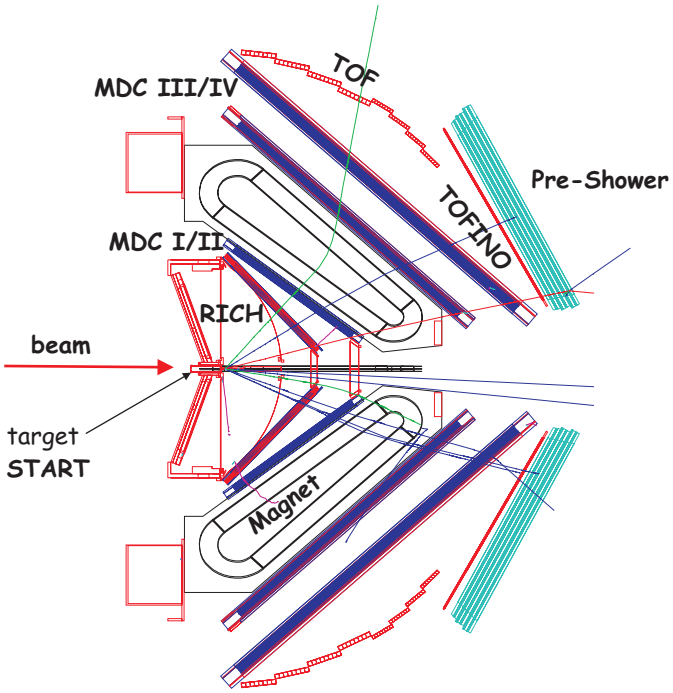

Fig. 1. Cut through two sectors of the HADES spectrometer, except for the magnet coils which are projected onto the cut plane to visualize the magnetic field. The average distance between the target and the outermost detectors is about 210 cm.

(M_{ch}) in the TOF detectors. (b) LVL2 is based on a real time identification of electron and positron candidates. All LVL2 trigger accepted events were written to tape, as well as a part of LVL1 (regardless of LVL2 decision) events (typically 10%) for normalization purposes, hadron analysis and check of the trigger performance. For the analysis presented here, only LVL1 trigger events were processed.

In the very first HADES physics run, the detector was operated using only the following sub-systems: the RICH, the two inner MDC planes, and the META, i.e. the two outer MDC planes were not operational and the coordi-

nate measurement of the META were used for tracking. In this mode the collision system $^{12}C + ^{12}C$ at 2A GeV was studied with a beam intensity of $I_{beam} = 10^6$ particles/sec impinging on a segmented carbon target with thickness $2 \cdot 2.5\%$ interaction length. $1.67 \cdot 10^7$ LVL1 triggered events with $M_{ch} \geq 4$ were analyzed in this study. In the event reconstruction, the track segments measured in the two inner MDC planes were correlated with hits in the META.

In the second data taking period the $^{12}C + ^{12}C$ system was studied at 1A GeV. Then, for the first time, a high-resolution tracking mode exploiting also the outer MDC planes was available. In this measurement, a carbon beam of 10^6 particles/sec was focused onto a carbon foil of 3.8% interaction length. $1.62 \cdot 10^7$ LVL1 triggered events with $M_{ch} \geq 4$ were used in this analysis.

3 Data Analysis

3.1 Simulation of acceptance

Artificial $^{12}C + ^{12}C$ events were generated with the UrQMD (v1.3b) transport code [12,13]. The detector response was simulated with the help of a Geant 3.21 based package [14] including the geometry and characteristics of all HADES detectors. The resulting raw data were processed in exactly the same way as the real data and used to quantify acceptance and efficiency corrections as well as systematic errors. Details on the different procedures are given in the corresponding subsections.

3.2 Momentum reconstruction

When traversing the spectrometer charged particles are deflected in the magnetic field, and at the same time they leave "hits" in the MDCs and META detectors. From this information together with the known magnetic field their trajectories are reconstructed and the momenta are deduced.

Two different tracking methods have been developed and were both used in the present analysis (see [5] for details). The first one is the "kickplane" algorithm which uses the position information delivered by the inner MDC chambers and the META system. In this case the momentum resolution σ_p/p, dominated by the limited position resolution of META, has been determined in simulations to be $\simeq 2\%$ at a momentum of 150 MeV/c, with a linear increase up to 22% at 1400 MeV/c. The second method is a Runge-Kutta based trajectory integration routine [15] which uses the information from all four MDC planes (with resolution $\sigma_p/p \simeq 3\%$). For the results presented in this paper, the kickplane method has been applied to the 2A GeV data, and both methods were used and compared for the 1A GeV data.

3.3 Particle identification

Particle identification in the HADES data analysis (for details see [5]) is based on Bayesian statistics [16,17]. The method allows to evaluate the probability that the reconstructed track can be related to a certain particle species (e.g. proton, kaon, π meson, electron, etc.). It combines

several observables from various sub-detectors (e.g. time of flight, energy loss) via probability density functions (PDF) determined for each observable and for all possible particle species. The probabilities for different mass assignments of any given track are calculated from the assumed abundances of the individual particle species and from the PDFs of all measured variables. The latter ones are obtained from simulations. If the assumed abundances differ significantly from the final results the procedure is repeated with updated input distributions. It converges typically after one or two iterations. The performance of the method in terms of efficiency and purity is evaluated in detailed simulations and simultaneous comparisons with the real data. In our case, hadron identification has been performed using measured momenta and corresponding velocities computed by means of the time-of-flight. For more sophisticated analyzes, like electron or rare hadron identification, data from the RICH and PreShower detectors as well as the energy loss in META and MDCs can be used in addition.

The method used for Particle IDentification (PID) is illustrated in Fig. 2 for the case of particle velocity (right) deduced from the measured time of flight and track length ("velocity-vs-momentum" algorithm). Particles with different masses occupy different regions in the velocity-vs-momentum distribution (left side); the pronounced ridges correspond to positive and negative pions, protons and deuterons. The Bayesian PID method requires the determination of the probability density functions for each particle species. In the case of the velocity-vs-momentum algorithm used here, the PDF is the probability distribution of velocity. For each type of particle it has been determined in bins of momentum and polar angle. In those velocity distributions gaussian fits were used to obtain the signal (i.e. particle yields) and a 2^{nd}-order polynomial fit to obtain the background (i.e. fake tracks). The fitted distributions were normalized to unity. Fig. 2 (right side) shows as an example of such fit for the momentum bin 350±5 MeV/c in the polar angle range $\theta = 60°\pm5°$.

Two quality parameters are used to characterize the performance of the method [18]: the PID efficiency and the PID purity. The PID efficiency $\varepsilon_t(p,\theta)$ is the probability that a particle with the true type t is identified as type t. The PID purity $\pi_t(p,\theta)$ is the probability that a particle that is identified as type t is truly of type t. The PID efficiency and purity have been studied in detailed simulations with events generated with the UrQMD model. The critical parameter here is the time resolution, which is well known. This limits the region in which we can use the method for π^+ and p identification to momenta < 1000 MeV/c because of the moderate time resolution of the presently installed TOFINO detectors. We have also checked that varying particle abundances even by a factor of 2 does not change the results significantly in the region of interest.

3.4 Total correction

Fig. 3 shows the dependences of the PID efficiency and purity on momentum for π^+, π^- and protons for the 2A GeV data in the TOFINO (right) and TOF (left) regimes. The

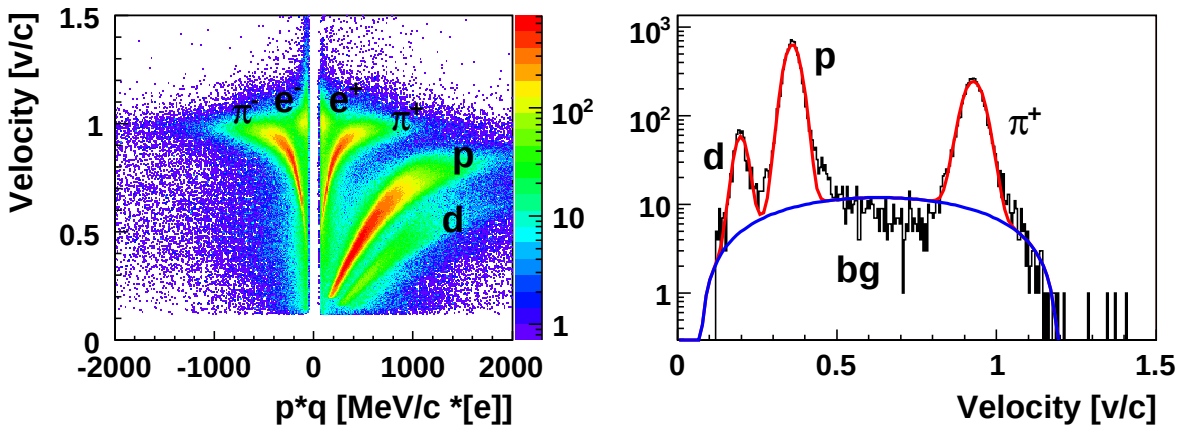

Fig. 2. Velocity vs. charge-times-momentum of charged particles as seen by the HADES detector from ^{12}C + ^{12}C collisions at 2A GeV (left). Projection onto the velocity axis of positively charged particles with momenta 350±5 MeV/c and $\theta = 60° \pm 5°$ (right). Fitted signal and background distributions are shown as lines.

efficiency of pion and proton identification is larger than 95% for all momenta in the TOF region. In the TOFINO region with its reduced time resolution the efficiency to identify positively charged pions drops steeply above 1000 MeV/c due to the ambiguity with the protons. The purity of pions (lower plots) does not reach unity because about 10% of the tracks identified as pions are due to muons from in-flight pion decays. A strong contamination of the positively charged pions with protons for momenta above 1000 MeV/c are again due to the low time resolution of TOFINO.

After the particle identification is done for all tracks, the resulting yields are corrected for efficiency and purity of the PID method, as well as for the detector and tracking efficiencies. The detection/tracking efficiency has also been obtained from Monte Carlo simulated and reconstructed UrQMD events. The total correction applied to the reconstructed particle yields reads

$$w_t(p,\theta) = \frac{\pi_t(p,\theta)}{\varepsilon_t(p,\theta) \times \varepsilon_t^{det}(p,\theta)}, \qquad (1)$$

where $\varepsilon_t^{det}(p,\theta)$, the detection efficiency, subsumes detector, track reconstruction and acceptance losses. It should be noted that we specify $\varepsilon_t^{det}(p,\theta)$ as function of θ and p, while averaging over the azimuthal angle. In this way, corrections for missing geometrical acceptance at some azimuthal angles (namely the spaces occupied by the six magnet coils) are accounted for as well as the losses due to pion in-flight decays.

Fig. 4 shows the dependence of the detection efficiency for $\pi^{\pm}$ and p as a function of momentum. The difference between proton and π efficiencies is again caused by the $\pi^{\pm}$ in-flight decay.

The total correction is applied to the data for each momentum and polar angle bin, and for each individual particle species. This is done only for bins with sufficiently high efficiency $\varepsilon_t^{det}(p,\theta) > 0.35$ in order to avoid large

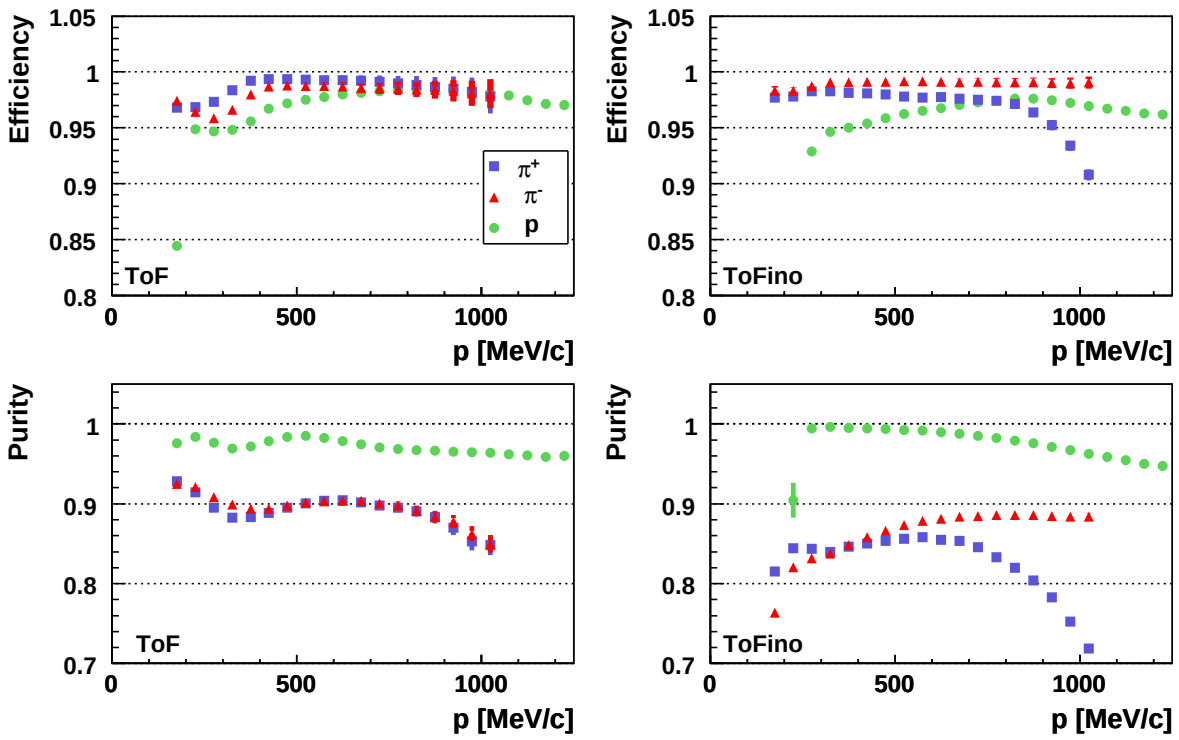

Fig. 3. Efficiency (top) and purity (bottom) of the PID method versus momentum for $\pi^{\pm}$ and protons in two sub-systems of the HADES detector: TOF (left) and TOFINO+PreShower (right) by using the kickplane reconstruction algorithm in ^{12}C + ^{12}C collisions at 2A GeV.

corrections at the sector boundaries. Data outside of this fiducial volume were excluded from further analysis.

Fig. 5 presents simulated polar distributions of pions in the center-of-mass system (cms). It shows the identified π^+ before and after applying the total correction, together with the primordial distribution delivered by the UrQMD model for 2A GeV ^{12}C + ^{12}C collisions. This self-consistency check quantifies $w_t(p, \theta)$ as a function of $\cos\theta_{cms}$ and demonstrates the wide coverage of our spectrometer. In Fig. 5 the angular anisotropy of pion emission in the UrQMD generator is clearly visible.

3.5 Event selection

For the present analysis, we used the HADES LVL1 trigger events, which are characterized by a hit multiplicity $M_{ch} \geq 4$ in the time-of-flight detectors. The correlation between the LVL1 trigger condition and the centrality of the reaction has been studied in Monte-Carlo simulation using the UrQMD and GEANT codes. Fig. 6 shows the simulated impact-parameter distributions. As for the "minimum bias" events corresponding to the total reaction cross section, we require in UrQMD at least one nuclear interaction (distribution marked by circles in Fig. 6). Then we pass these events through our analysis code and require that they fulfill the LVL1 condition (triangles in

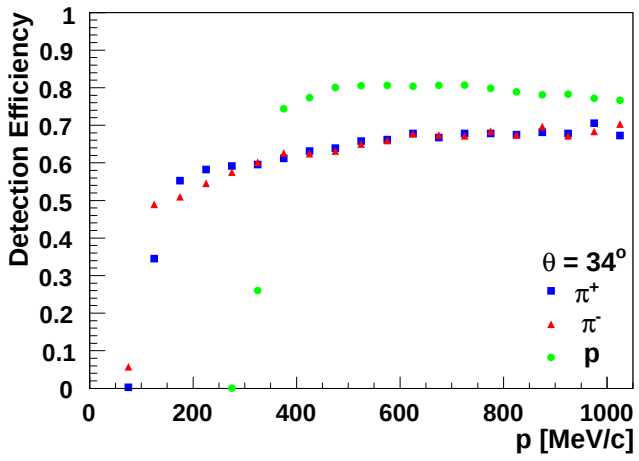

Fig. 4. The detection efficiency $\varepsilon_t^{det}(p,\theta)$ vs. momentum for $\pi^{\pm}$ and protons using the kickplane reconstruction in ^{12}C+^{12}C collisions at 2A GeV.

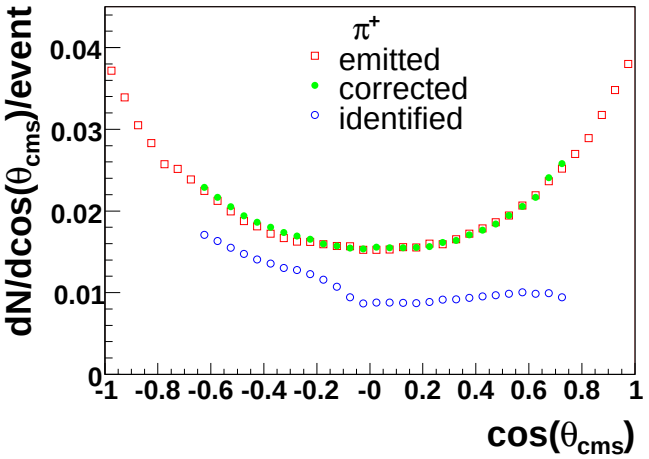

Fig. 5. Center-of-mass polar angle distributions of π^+. The squares represent the pions as generated by UrQMD. Only π mesons with $p_{cms} > 200 MeV/c$ have been selected. The open circles show those generated pions which are detected and identified in the HADES acceptance. The full circles depict the result of the efficiency and purity correction to the accepted pions.

Fig. 6). We found that the LVL1-triggered events correspond to 52% and 60% of the total reaction cross section in ^{12}C + ^{12}C collisions at 1 and 2A GeV, respectively. As we did not find a straightforward way how to extract the average number of participants for our trigger biased events, we proceeded in the following way. For a minimum bias events the average number of participating nucleons was estimated from the geometrical model [19]. In our case of symmetric collisions systems the average number of participants is $\langle A_{part}\rangle = A/2 = 6$. We deduce the mean $\langle A_{part}\rangle$ for reactions accepted by LVL1 by comparing the pion multiplicity of UrQMD for LVL1 accepted events to minimum bias events and using $\langle A_{part}\rangle$ scaling of pion production, i.e. $6 \cdot \langle M_\pi^{LVL1}\rangle / \langle M_\pi^{min.b.}\rangle$. The LVL1 trigger effect is significant, and the number of participants increases by $\approx 40\%$. The average impact parameters, the average pion multiplicities and average number of participants from UrQMD are listed in Tab. 1, for the true minimum-bias events and after applying LVL1 trigger at both 1 and 2A GeV.

The distributions of the number of reconstructed tracks per LVL1 event of data and UrQMD simulations are in a reasonable agreement, as shown in Fig. 7. This is another confirmation that the modelling of the detector and tracking efficiency as well as of the LVL1 event selection in our simulation is realistic concerning the charged particle multiplicity and thus the trigger selection and cross section.

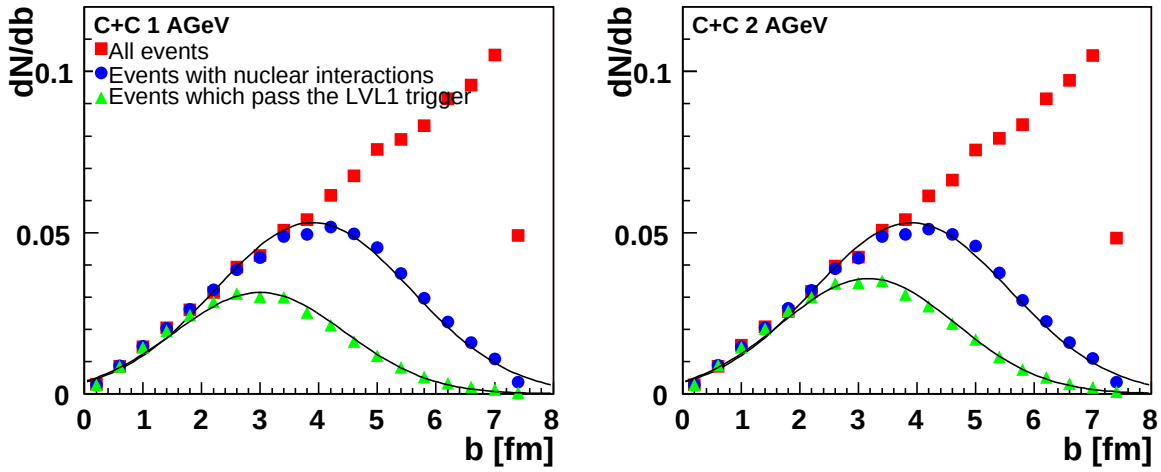

Fig. 6. The impact parameter distribution obtained from the UrQMD model for ^{12}C + ^{12}C collisions at 1 (left) and 2A GeV (right).

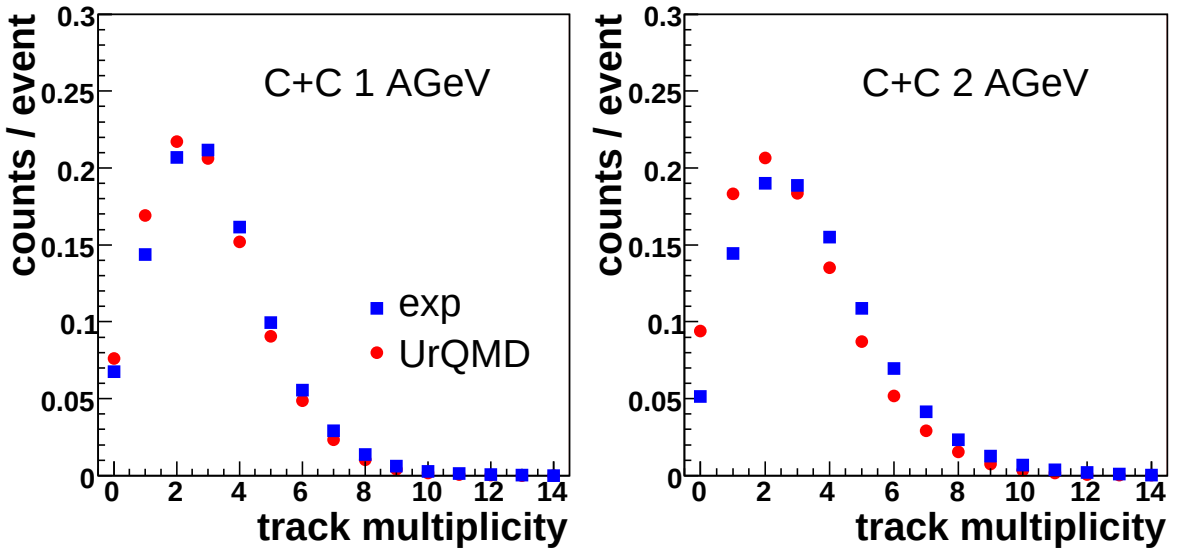

Fig. 7. Distribution of the number of reconstructed tracks in the data and in the simulation for 1 (left) and 2A GeV (right) ^{12}C + ^{12}C collisions.

4 Results

4.1 Transverse-mass distributions

Figures 8 and 9 exhibit the measured and simulated transverse mass distributions of π^+ and π^- in different intervals of normalized rapidity $y_0 = (y_{lab} - y_{cms})/y_{cms}$ for ^{12}C+^{12}C at 1A GeV and 2A GeV, respectively. The systematic errors of the data are estimated from the differences between distributions from the 6 independent HADES sectors as 5%. The transverse-mass ($m_\perp$) distributions have been fitted for each rapidity bin using one or two

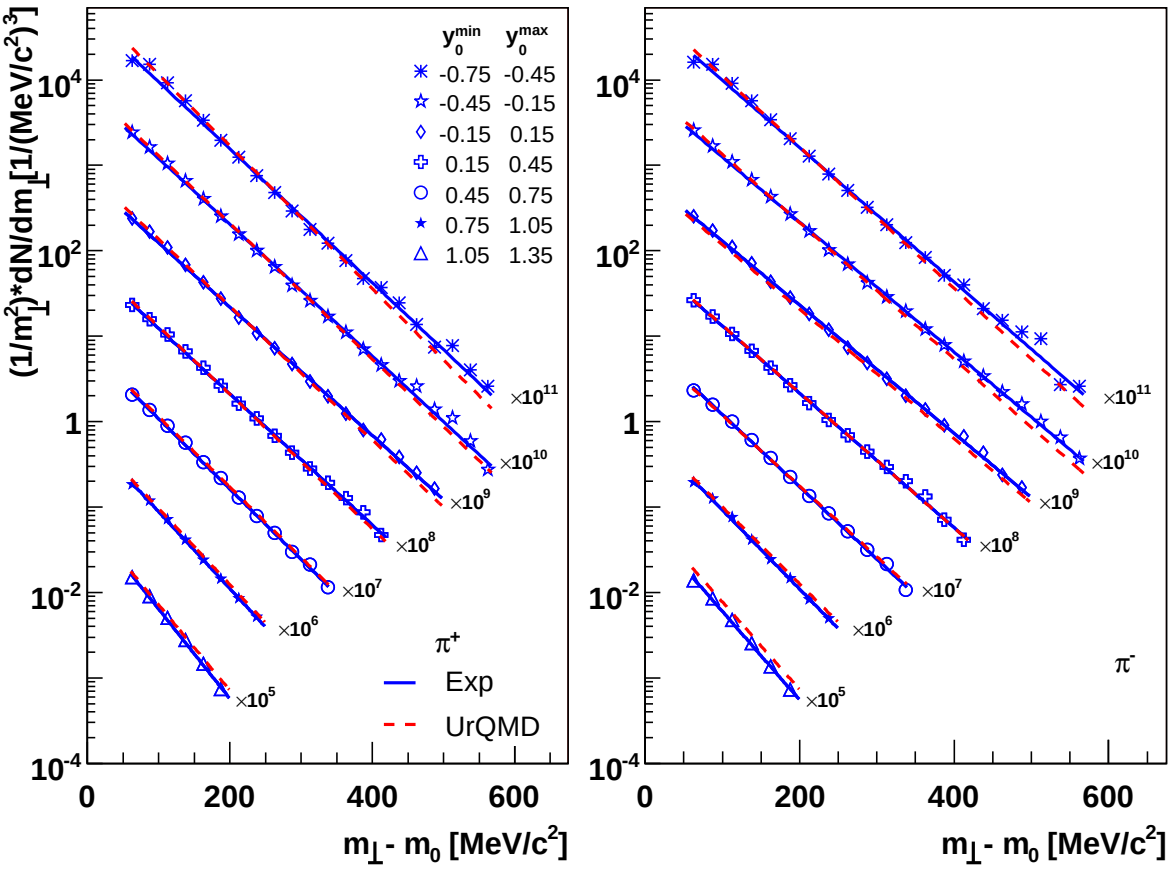

Fig. 8. Transverse-mass distributions for positive (left) and negative (right) pions in different slices of rapidity derived from the data in ^{12}C + ^{12}C collisions at 1A GeV. Full lines show the results of fits of the data using one exponential function, while dashed lines show fits of the UrQMD distributions using the same fit function. Error bars (systematic and statistical ones) are not visible at this scale.

exponential functions. The fit with two slopes employs

$$\frac{1}{m_\perp^2}\frac{dN(y)}{dm_\perp} = C_1(y)\,\exp\left(-\frac{m_\perp}{T_1(y)}\right) + C_2(y)\,\exp\left(-\frac{m_\perp}{T_2(y)}\right) \quad (2)$$

with $m_\perp = (p_\perp^2 + m^2)^{1/2}$, and $p_\perp$ as transverse momentum; $C_{1,2}$ are normalizations and $T_{1,2}$ the inverse slope parameters. It describes the experimental data better than a fit with one slope (i.e., $C_2 \equiv 0$) for the 2A GeV data sample (χ^2/ndf around 1.0 vs. 4.8 for the fit with one exponential).

Fig. 8 clearly demonstrates that for the lower bombarding energy of 1A GeV, a fit with one slope is sufficient for the description of the spectral shape. The inverse-slope parameters for both pion species at mid-rapidity for 1A GeV (-0.15 $\leq y_0 \leq$ 0.15) and 2A GeV (-0.1 $\leq y_0 \leq$ 0.1) are summarized in Tab. 2 using one and two exponential functions. The slopes of π^+ and π^- agree within error bars for the single exponential fit, while the two-exponentials fit the π^+ spectrum at 1A GeV appear flatter than the π^- spectrum. At 2A GeV, UrQMD predicts different spectral

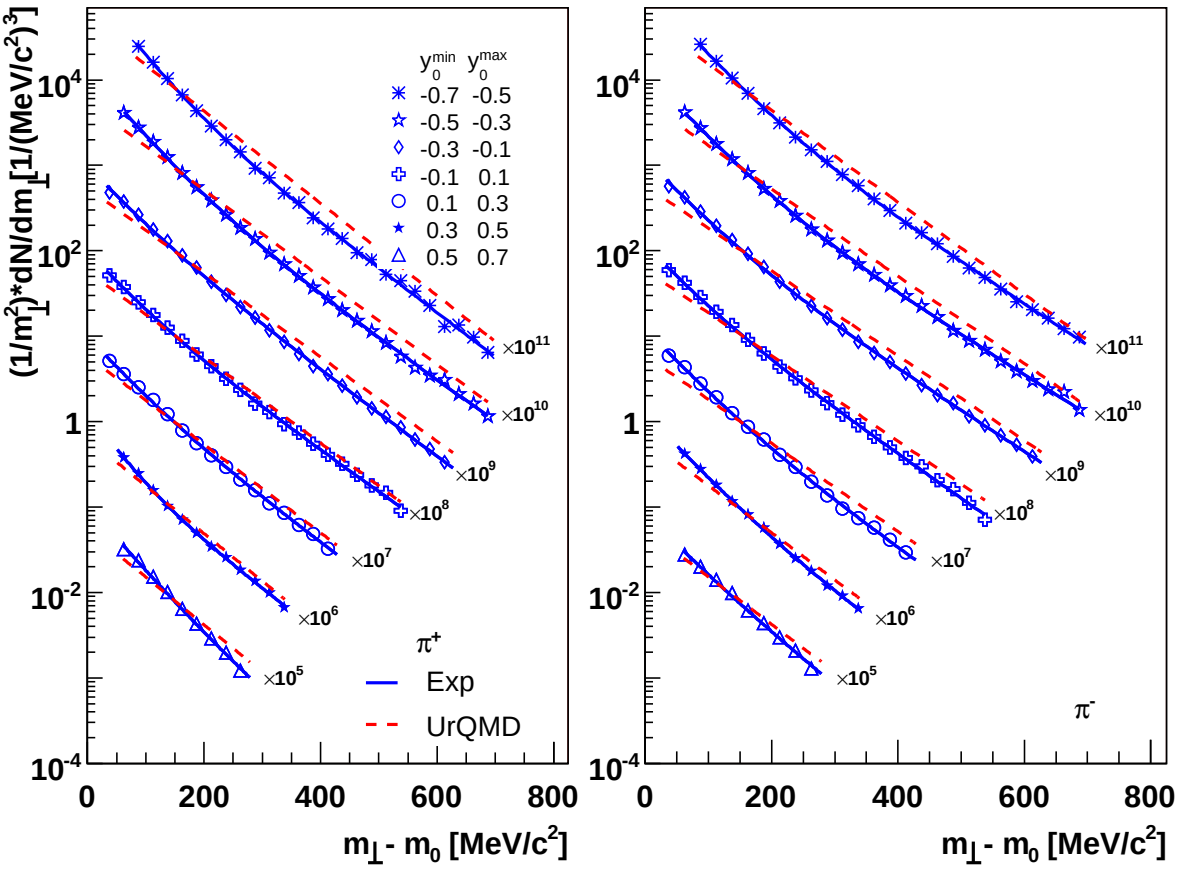

Fig. 9. Transverse-mass distributions for positive (left) and negative pions (right) in different slices of rapidity derived from the data in ^{12}C + ^{12}C collisions at 2A GeV. Full lines show the results of fits of the data using two exponential functions, while dashed lines show fits of the UrQMD distributions using one exponential function. Error bars (systematic and statistical ones) are not visible at this scale.

shapes (flatter spectra), while at 1A GeV agreement of UrQMD with data is better.

Similar values for the inverse slopes have been extracted from previous experiments on charged pion production in ^{12}C + ^{12}C collisions by the KaoS collaboration [1,20], and for neutral pions at 1 and 2A GeV by the TAPS collaboration [21]. One has to be aware of the fact that this comparison of the slope values of different experiments has a limited relevance due to the different acceptances (valid mainly for the comparison with the KaoS data) and also conditions of the fit itself. Still it is apparent that the transverse mass distributions measured by all three experiments are fairly similar. At 1A GeV, the slope parameters for the two-exponential fit agree well with KaoS data for $\pi^{\pm}$, and for the single exponential fit we find also good agreement with TAPS data for π^0. At 2A GeV, however, our soft component described by T_1 in the two-exponential fit is systematically larger than the corresponding parameter deduced by KaoS. In contrast,

Table 2. Inverse slope parameters for $\pi^{\pm}$ measured at mid-rapidity derived from the data (using one and two exponential functions) and UrQMD (using one exponential function) in ^{12}C + ^{12}C collisions at 1 and 2A GeV, in units of MeV.

Beam energy = 1A GeV						
Particle	Data				UrQMD	
	T (2 slopes)	χ^2/ndf	T (1 slope)	χ^2/ndf	T (1 slope)	χ^2/ndf
π^+	49.5 ± 0.1; 69.5 ± 1.9	0.61	57.8 ± 0.3	1.7	55.4 ± 0.3	2.2
π^-	40.3 ± 7.5; 60.7 ± 0.3	1.0	57.9 ± 0.3	1.4	55.4 ± 0.3	2.0
Beam energy = 2A GeV						
Particle	Data				UrQMD	
	T (2 slopes)	χ^2/ndf	T (1 slope)	χ^2/ndf	T (1 slope)	χ^2/ndf
π^+	47.7 ± 6.2; 90.6 ± 3.3	0.9	80.9 ± 0.5	4.7	86.5 ± 0.6	1.5
π^-	46.4 ± 5.2; 84.4 ± 2.1	1.2	76.7 ± 0.5	4.9	86.7 ± 0.6	1.4

the single-exponential slope parameters for $\pi^{\pm}$ compares well with the one reported by TAPS for π^0.

Other fits of the transverse-momentum distributions are conceivable. For instance, a blast wave fit (see [22] for the formula) is possible, however if applied to only one particle type it does not allow for the unambiguous determination of a flow parameter.

4.2 Rapidity distributions

As seen in the previous chapter, the HADES acceptance in $p_\perp$ is rather large. For the missing parts of the acceptance at low and high $p_\perp$ we extrapolated the yield. In doing so, for each slice centered at rapidity y the corresponding $p_\perp$ distribution was fitted by the function

$$\frac{1}{p_\perp^2}\frac{dN}{dp_\perp} = c_1(y)\exp\left(-\frac{p_\perp}{T_1(y)}\right) + c_2(y)\exp\left(-\frac{p_\perp}{T_2(y)}\right). \quad (3)$$

These fit results were used to estimate the $\pi^{\pm}$ yield outside the acceptance. The resulting correction were $\approx 5\%$ and $\approx 2\%$ for π^+ and π^- respectively, except for data at the border of the rapidity acceptance, where the correction was 10 - 20 %. Fig. 10 shows the rapidity distributions obtained by integration of the extrapolated $p_\perp$ spectra of π^+ and π^- for ^{12}C + ^{12}C at 1 and 2A GeV for the data. UrQMD simulations are also displayed. Additionally, we simulated the rapidity distribution using a simple Monte-Carlo event generator PLUTO [23], which

Table 1. Average impact parameters, pion multiplicities, and average number of participating nucleons from UrQMD calculations for ^{12}C + ^{12}C at 1 and 2A GeV before and after applying the LVL1 trigger condition.

Beam energy = 1A GeV				
	$\langle b \rangle$	$\langle M_{\pi+} \rangle$	$\langle M_{\pi-} \rangle$	$\langle A_{part} \rangle$
minimum-bias events	3.95 fm	0.36	0.36	6
LVL1 triggered	3.01 fm	0.51	0.52	8.61
Beam energy = 2A GeV				
	$\langle b \rangle$	$\langle M_{\pi+} \rangle$	$\langle M_{\pi-} \rangle$	$\langle A_{part} \rangle$
minimum-bias events	3.95 fm	0.83	0.83	6
LVL1 triggered	3.18 fm	1.15	1.17	8.38

assumes a thermal source modified by a polar angular distribution (see below). The used simulation parameters - inverse slopes and anisotropies - were derived from our data, and we normalized the resulting distribution to the measured data (π^+ and π^- averaged), see Fig. 10.

The distributions exhibit a Gaussian-like shape with a standard deviation (σ referring to the scaled rapidity y_0) of about 1.0 for both systems. In the case of the 1A GeV data, the experimental rapidity distribution is about by 20% narrower than the simulated one. This is in agreement with the finding (see section 4.4 below) that the anisotropy parameter has a lower value in the experimental data than in UrQMD simulation. Note for the 2A GeV case a slight underestimation of our data by UrQMD.

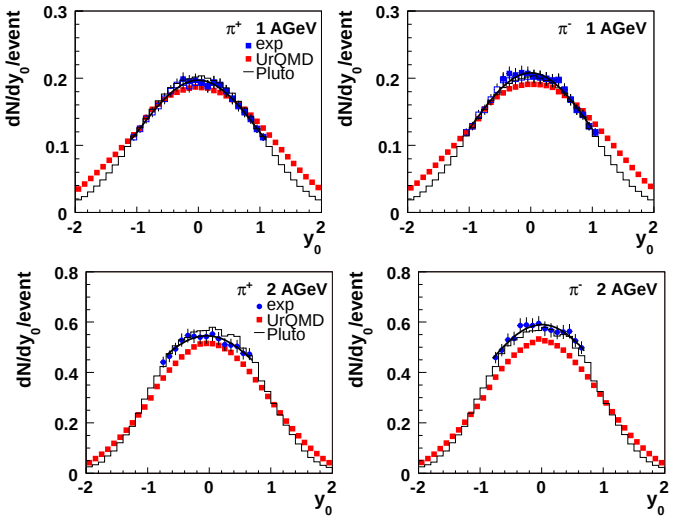

Fig. 10. The rapidity distribution of positive (left) and negative (right) pions produced in ^{12}C + ^{12}C collisions at 1A GeV (top) and 2A GeV (bottom). Circles with error bars show data, while full squares depict UrQMD calculations. The distributions obtained by the PLUTO generator are shown by histograms normalized to the measured yields (with π^+ and π^- averaged). In the 1A GeV case, the data points reflected from forward rapidities are shown as open symbols. The slight asymmetries of dN/dy with respect to inflection at $y_0 = 0$ are used to control the systematic errors.

4.3 Multiplicities

Pion yields N_π per reaction (LVL1 trigger condition) within the HADES acceptance region as shown in Fig. 10 and in full phase space resulting from two extrapolation methods A and B are presented in Tab. 3. The method A is based on the UrQMD model whereas the method B uses the PLUTO model described above (see distributions in Fig. 10). It is expected that the transport model describes the meson production better than a simple thermal pro-

Table 3. Particle yields per reaction (LVL1 trigger condition) of $\pi^{\pm}$ from $^{12}C + ^{12}C$ collisions. N_π means the measured yield, while $N_\pi(4\pi)$ denotes the 4π extrapolated yield, either using method A or B. The statistical errors are negligible, and the systematic errors are discussed in the text.

Beam energy = 1A GeV			
Particle	N_π	$N_\pi(4\pi$, A)	$N_\pi(4\pi$, B)
π^+	0.36	0.51	0.46
π^-	0.38	0.54	0.49
Beam energy = 2A GeV			
Particle	N_π	$N_\pi(4\pi$, A)	$N_\pi(4\pi$, B)
π^+	0.77	1.28	1.19
π^-	0.82	1.37	1.28

duction implemented in PLUTO. Below we use the results obtained by method A. The differences between the two methods are estimates of the systematic errors of the yield extrapolations.

Using the estimated averaged number of participants in the LVL1 triggered events (see in Tab. 1), the resulting $\pi^{\pm}$ multiplicity per participant (averaged for π^+ and π^-) is then 0.061 ± 0.007 and 0.158 ± 0.017 at 1 and 2A GeV, respectively. The systematic error of the yields is estimated to be 11%; it is the sum of uncertainties connected with the efficiency/purity corrections, the extrapolation to full solid angle and full kinematic phase space, and the determination of the number of participating nucleons.

The obtained values can be compared to the results published previously for the same systems and energies by the TAPS [21] and KaoS [20] collaborations. Both former experiments did not measure the pion multiplicities, but the minimum-bias pion production cross section in a restricted part of momentum space and polar angle (in the case of TAPS only at mid-rapidity, and in the case of KaoS at 2A GeV only at the laboratory polar angle of 40°). In order to compare these data with our results we made two steps: First, we calculated the pion multiplicities per participant from the published production cross sections dividing them by the total reaction cross section 0.95 b (calculated according to $\sigma = \pi r_0^2 (A_p^{1/3} + A_t^{1/3})$ assuming $r_0 = 1.20 fm$), and the average number of participants for minimum bias events, 6. The second step is a correction on the polar anisotropy. For the TAPS data at both energies, and KaoS data at 2A GeV, the cross section to full phase space was extrapolated assuming isotropic emission. In this study, however, we have measured the pion angular distribution and found a strong polar anisotropy (see next subsection). Therefore, we corrected these data, using the anisotropy coefficient $A_2 = 0.5$ and 0.7 (see formula (4) below) for 1A GeV (TAPS) and 2A GeV (TAPS and KaoS). Tab. 4 shows a comparison of all measured π meson multiplicities per participant and results of our UrQMD simulations as well.

As seen in Tab. 4 our results are very consistent with the TAPS as well as KaoS data. Due to rather large errors, it is difficult to draw any conclusion about the difference in production of neutral and charged π mesons as predicted by UrQMD.

Table 4. Comparison of multiplicities per participant of π mesons derived from our data and previous experiments from ^{12}C + ^{12}C collisions at 1 and 2A GeV together with UrQMD results.

Beam energy = 1A GeV				
Particle	this work	KaoS [20]	TAPS [21]	UrQMD
π^+		0.061 ± 0.009		
$1/2(\pi^+ + \pi^-)$	0.061 ± 0.007			0.059
π^0			0.059 ± 0.005	0.067
Beam energy = 2A GeV				
Particle	this work	KaoS [20]	TAPS [21]	UrQMD
π^+		0.158 ± 0.014		
$1/2(\pi^+ + \pi^-)$	0.158 ± 0.017			0.137
π^0			0.154 ± 0.015	0.159

4.4 Angular distributions

The measured centre-of-mass polar angular distributions of pions produced in 1 and 2A GeV ^{12}C + ^{12}C collisions are exhibited in Fig. 11. Pions with centre-of-mass momenta between 200 and 800 MeV/c have been selected. No losses in acceptance occur in this phase space region for the polar angles range shown in Fig. 11. The systematic errors of the data are again estimated from the differences between distributions from the six independent HADES sectors to be 5%.

In the symmetric collision system ^{12}C + ^{12}C the polar angle distributions in the center-of-mass system can be fitted with the following expression

$$\frac{dN}{d(\cos\theta_{cms})} = A_1(1 + A_2\cos^2\theta_{cms}). \qquad (4)$$

The fit parameter A_2 characterizes the anisotropy of the pion source, and A_1 is a normalization. As visible in Fig. 11, the data show very strong anisotropies quantified by $A_2 = 0.88\pm0.12$ and 1.19 ± 0.16 for beam energies of 1 and 2A GeV. The UrQMD model gives also a quite strong anisotropy with $A_2 = 1.45$ and $A_2 = 1.12$ ($A_2 = 0.56$ and $A_2 = 0.70$ when integrated over all momenta including also the region outside our acceptance).

We observe a strong dependence of the anisotropy on momentum. This is evident from Fig. 12, where A_2 is displayed as a function of the pion's centre-of-mass momentum from fits to our data.

One can see that the anisotropy steadily increases with momentum for both pion species and both beam energies up to $A_2 \simeq 1.0 - 1.5$, around 400 MeV/c, where it has

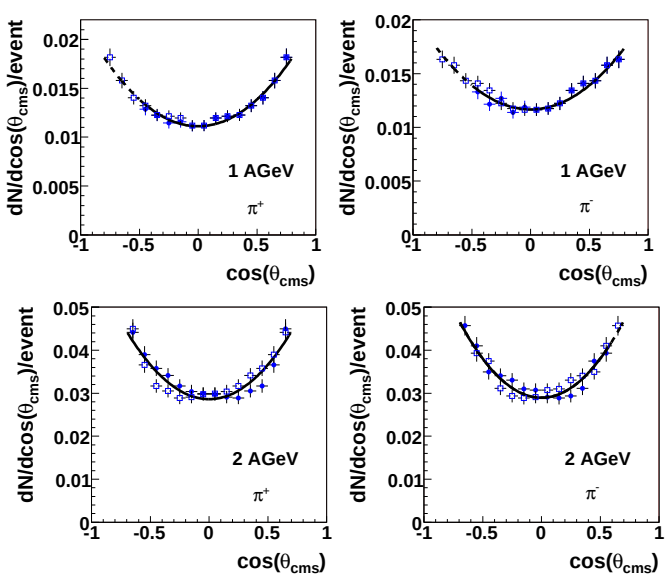

Fig. 11. Polar distribution in the center-of-mass system of positive (left) and negative (right) π mesons produced in ^{12}C + ^{12}C collisions at 1A GeV (top) and 2A GeV (bottom). Full circles show measured data. The data points reflected around 90° are shown as open squares. The lines show the fit by formula (4). Pions with momenta 200 - 800 MeV/c have been selected.

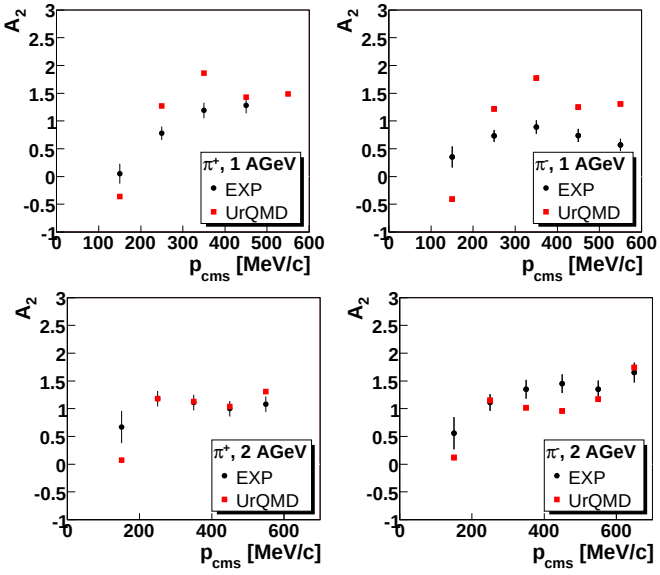

Fig. 12. Dependence of the anisotropy parameter A_2 on the momentum in the center-of-mass system for positive (left) and negative (right) pions produced in ^{12}C + ^{12}C collisions at 1A GeV (top) and 2A GeV (bottom). Circles with error bars show fits to data, while squares exhibit fits to UrQMD simulations after the full analysis chain.

a tendency to level off. This behavior is fairly well reproduced by the UrQMD model, which, however, tends to level off at somewhat larger values (see Fig. 12). For the data in the region 100 MeV/c $< p_{cms} <$ 200 MeV/c, the anisotropy can still be fitted in a limited Θ_{cms} range. The results show significantly lower anisotropy parameters for both the data and UrQMD. The close to zero (at 2A GeV) and even slightly negative anisotropies given by UrQMD for low momenta at 1A GeV are not seen in the experiment.

It is interesting to compare these distributions to the corresponding ones for $NN \rightarrow N\Delta \rightarrow NN\pi$ reactions which are expected to be the dominant source of the pion production at these energies [2,3]. In order to estimate them we have used our PLUTO generator employing measured Δ distributions [24]. It turns out that the shape of the A_2 distributions is similar but the corresponding distributions level-off at substantially higher values: about 3.5 and 5 for 1 and 2A GeV, respectively. This can be considered as hint to collectivity due to re-scattering and final state interactions even in the small system under consideration here.

Before the present work no data had been published on pion anisotropies in ^{12}C + ^{12}C collisions. Early studies of pion production in Ne-induced reactions at 0.8A GeV on NaF, Cu and Pb targets had found almost isotropic angular distributions for very low pion cms kinetic energies ($E_{\pi^+} \leq 50$ MeV), but substantial anisotropies for all higher energies ($E_{\pi^+} \geq 150$ MeV) [25]. The two closest systems studied most comprehensively in this respect are, however, 0.8 as well as 1.8A GeV Ar+KCl [26,27] and 1.93A GeV Ca+Ca [4]. While in both cases similar momentum-averaged anisotropies were observed, with values of $\langle A_2 \rangle = 0.5 - 0.6$, only the Ar+KCl data display a strong pion-energy dependence of A_2, peaking around E_π = 200-300 MeV. Based on a comparison with transport calculations, the authors of Ref. [4] attributed these differences to the very different centralities covered by their measurement. As seen from Fig. 12 and as discussed above, we do not observe in C+C, at both bombarding energies, a rise and fall of A_2, but rather a simple levelling-off with increasing pion cms momenta.

5 Summary

In summary, the charged pion characteristics in the reaction ^{12}C + ^{12}C at 1 and 2A GeV has been measured with the HADES spectrometer. The measured π meson yields are in agreement with previous results for the same systems and energies measured by the TAPS and KaoS detectors.

Our data on the pion transverse mass distributions at mid-rapidity can be described by a Maxwell-Boltzmann function for 1A GeV, while the 2A GeV data show a strong second exponential component with lower slope. This finding is in agreement with former results for the same system and energy for $\pi^\pm$ [20], whereas π^0 data [21] exhibit only one slope distribution. Reasonable agreement of our transverse momentum spectra at both energies with UrQMD calculations indicate that the degree of thermalization in the light C+C system is adequately reproduced in the model.

In contrast to older data which were measured in a limited angular range, strong pion anisotropies have been observed in the much larger acceptance region of the present experiment. The systematics [4] of pion production in heavier systems at comparable beam energies points to similar anisotropy values as extracted from our data sample. The asymmetries have a non-trivial momentum dependence. A peaking of the asymmetry as reported in [26], however, can not be confirmed. Our results are largely in agreement with the UrQMD transport model. From comparison of our results with the pp data follows that the observed anisotropies can be caused by remnants of the intrinsic behavior of the underlying inelastic NN scattering which involves Δ excitation.

Acknowledgments

The HADES collaboration gratefully acknowledges the support by BMBF grants 06MT238, 06TM970I, 06GI146I, 06F-140, 06FY171, and 06DR135, by DFG EClust 153 (Germany), by GSI (TM-KRUE, TM-FR1, GI/ME3, OF/STR), by grants GA AS CR IAA100480803 and MSMT LC 07050

(Czech Republic), by grant KBN 5P03B 140 20 (Poland), by INFN (Italy), by CNRS/IN2P3 (France), by grants MCYT FPA2006-09154, XUGA PGID IT06PXIC296091PM and CPAN CSD2007-00042 (Spain), by grant FTC POCI/FP /81982 /2007 (Portugal), by grant UCY-10.3.11.12 (Cyprus), by INTAS grant 06-1000012-8861 and EU contract RII3-CT-2004-506078.

References

1. P. Senger and H. Ströbele, J. Phys. G 25, R59 (1999).
2. A.B. Larionov and U. Mosel, Nucl. Phys. A 728, 135 (2003);
   S. Teis et al., Z. Phys. A 356, 421 (1997).
3. A. Engel, A.K. Dutt-Mazumder, R. Shyam, U. Mosel, Nucl. Phys. A 603, 387 (1996).
4. W. Reisdorf et al. (FOPI collaboration), Nucl. Phys. A 781, 459 (2007).
5. R. Schicker et al. (HADES collaboration), Nucl. Instr. Meth. A 380, 586 (1996).
   G. Agakishev et al. (HADES collaboration), to be published.
6. G. Agakishev et al. (HADES collaboration), Phys. Rev. Lett. 98, 052302 (2007).
7. G. Agakishev et al. (HADES collaboration), Phys. Lett. B 663, 43 (2008).
8. A. Balanda et al., Nucl. Instr. Meth. A 531, 445 (2004).
9. C. Agodi et al., Nucl. Instr. Meth. A 492, 14 (2002).
10. J. Lehnert at al., Nucl. Instr. Meth. A 502, 261 (2003).
11. A. Toia et al., Nucl. Instr. Meth. A 502, 270 (2003).
12. S.A. Bass et al., Prog. Part. Nucl. Phys. 41, 225 (1998).
13. M. Bleicher et al., J. Phys. G 25, 1859 (1999).
14. R. Brun et al., GEANT3 users guide, CERN-DD/EE/84-1 (1987).
15. W.H. Press, S.A. Teukolski, W.T. Vetterling, and B.P. Flannery, "Numerical Recipies", 4th edition, Cambridge University Press (2007).
16. A. Stuart and A.K. Ord, "Kendall's Advanced Theory of Statistics", Vol. I. Distribution Theory 5th Ed. (Oxford University Press, New York, 1987).
17. R. Barlow et al., *Recommended Statistical Procedures for BABAR*, BABAR analysis document No.318, (2002), www.slac.stanford.edu/BFROOT/www/Statistics/Report/report.pdf.
18. B. Hommez, Nucl. Instr. Meth. A 502, 294 (2003).
19. J. Gosset et al., Phys. Rev. C 16 (1977) 629;
    J. Hüfner and J. Knoll, Nucl. Phys. A 290, 460 (1977).
20. F. Laue et al. (KaoS Collaboration), Eur. Phys. J. A 9, 397 (2000);
    C. Sturm, PhD thesis, TU Darmstadt, 2001.
21. R. Averbeck et al. (TAPS Collaboration), Phys. Rev. C 67, 024903 (2003).
22. K. Adcox et al. (PHENIX collaboration), Phys. Rev. C 69, 024904 (2004).
23. I Fröhlich et al. (HADES collaboration), arXiv:0708.2382 [nucl-ex].
24. V. Dmitriev, O. Sushkov, C. Gaarde, Nucl. Phys. A 459, 503 (1986).
25. J. Chiba et al., Phys. Rev. C 20, 1332 (1979).
26. R. Brockman et al., Phys. Rev. Lett. 53, 2012 (1984).
27. S. Nagamiya et al., Phys. Rev. C 24, 971 (1981).